A 60 GHz PCB Wideband Antenna-in-Package for 5G/6G Applications

Lidong Chi, *Student Member, IEEE*, Zibin Weng, *Member, IEEE*, Yihong Qi, *Senior Member, IEEE*, and James L. Drewniak, *Fellow, IEEE*

***Abstract*—A low-cost, wideband printed circuit boards (PCBs) manufactured antenna is proposed in this letter for 5G/6G antenna-in-package (AiP) applications with wideband common-mode current (surface-wave) choking characteristics. The antenna is based on a grounded, wideband, high-efficiency electromagnetic structure (WHEMS) and a backing cavity, in which a radiating choke is introduced. By changing the choking condition of a quarter-wave length, widely applied in traditional low-frequency baluns, wideband common-mode current suppression is achieved. The enclosing wall of the backing cavity is realized by a combination of isolated grounded vias and connected grounded vias based on current polarization on the wall. Finally, a 22% impedance bandwidth (60–75 GHz) and a relative gain of 8–10 dBi within the band is achieved.**

***Index Terms*—5G, 6G, antenna-in-package (AiP), common-mode current, printed circuit boards (PCBs), surface wave.**

I. Introduction

NOWADAYS, 5G commercialization has started in quite a few countries, and some preliminary 6G research has already been initiated [1]. Antenna systems are critical components for 5G/6G communication systems [2], [3]. The recent antenna-in-package (AiP), which provides compact antenna and packaging solutions for 5G/6G communication systems, is widely used in applications of 60 GHz and above, such as wireless communications, phased arrays, automotive radar, and sensors [4]–[7]. Considering the performance, cost, and volume of antennas, wireless systems are becoming more compact due to AiP, where the physical distance between antennas and the system becomes unprecedentedly close [8], [9]. The compactness results in a small form factor, but introduces electromagnetic interference caused by common-mode currents. The common-mode current, i.e., those currents on unintended portions of the conducting structures, can be problematic, which not only changes the radiating characteristics of the antenna from the designed characteristics, but also couples noise from the system when it runs through a noisy part of the system [10], [11]. Due to the short coupling distance, high material dielectric constant, and limitations in processing of low-temperature cofired ceramics (LTCC) and printed circuit boards (PCBs), design with common-mode current suppression in AiP applications is challenging [12], [13].

Common-mode currents primarily come from two sources, which are the residual currents on unintended portions of the feed or packaging structure caused by unbalanced feeding arrangements, and the surface-wave [14], [15]. Previous work has been reported for minimizing the common-mode currents in AiP applications. In [16], the surface-wave between adjacent array elements was suppressed by LTCC-based metal walls (MWs), which are higher than the radiating surface to reduce coupling between elements of the array. In [17], a substrate-integrated waveguide (SIW) slot antenna was introduced, the shielding wall of which was realized by plated square grooves arranged discontinuously in a line. However, additional fabrication processes, which increase the manufacturing complexity, cost, and risk of structure deformation, were required in these methods. A uniplanar compact electromagnetic band-gap (UC-EBG) structure was proposed in [18] to decrease the mutual coupling caused by the surface-wave in 60 GHz LTCC applications. The UC-EBG is a periodic electromagnetic structure, which requires large dimensions to realize a common-mode current suppression, and is put outside the array with no effect on mutual coupling between elements. A soft surface was used in [19] to suppress the common-mode current. The choking structure occupies one unit of space, but the currents on it give nearly no contribution to the main radiation, which will decrease the aperture efficiency. Compared with [19] and [20] proposed a more compact soft surface. However, using an L-probe-fed patch antenna, imbalance is observed in the simulated current distributions of [20].

In this letter, a wideband directional antenna is proposed with common-mode current suppression characteristics. The antenna is evolved from a wideband, high-efficiency electromagnetic structure (WHEMS), which is widely used in low-frequency applications for its balanced structure, and wideband, high gain properties [21]–[24]. Through improvement of a quarter-wave transformer, a radiating choke is introduced, not only suppressing the common-mode currents, but also having currents that

Manuscript received May 29, 2020; accepted June 21, 2020. Date of publication July 3, 2020; date of current version November 23, 2020. This work was supported in part by the Chinese Ministry of Education China Mobile Research Foundation under Grant MCM 20150101 and in part by the National Natural Science Foundation of China under Grant 61671203. *(Corresponding author: Zibin Weng.)*

Lidong Chi is with Hunan University, Changsha 410082, China, and also with General Test Systems, Inc., Shenzhen 518000, China (e-mail: 565548254@qq.com).

Zibin Weng is with Xidian University, Xi'an 710071, China (e-mail: zibinweng@mail.xidian.edu.cn).

Yihong Qi is with the Peng Cheng Laboratory, Shenzhen 518066, China, also with the General Test Systems, Inc., Shenzhen 518102, China, also with Hunan University, Changsha 410082, China, also with the Missouri University of Science and Technology, Rolla MO 65409 USA, and also with Western University, London, ON N6A 3K7, Canada (e-mail: qiyh@pcl.ac.cn).

James L. Drewniak is with the EMC Laboratory, Missouri University of Science and Technology, Rolla, MO 65401 USA (e-mail: drewniak@mst.edu).

Digital Object Identifier 10.1109/LAWP.2020.3006873

1536-1225 © 2020 IEEE. Personal use is permitted, but republication/redistribution requires IEEE permission.
See https://www.ieee.org/publications/rights/index.html for more information.

Authorized licensed use limited to: HUNAN UNIVERSITY. Downloaded on March 04,2021 at 08:47:05 UTC from IEEE Xplore. Restrictions apply.

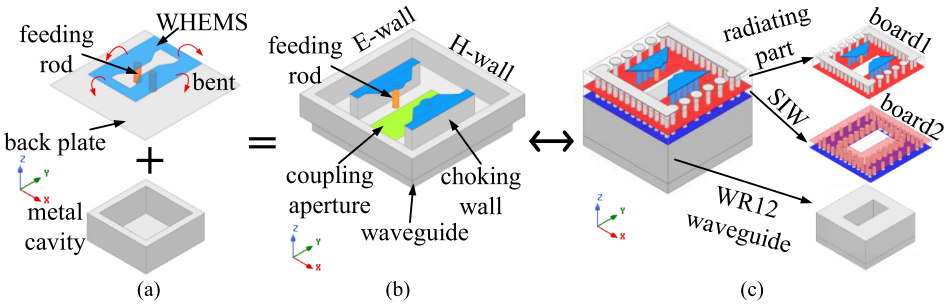

Fig. 1. Evolution of the proposed antenna. (a) WHEMS with a back plate and metal backing cavity. (b) Ideal model of the proposed antenna. (c) AiP implementation of the proposed antenna in PCB technology.

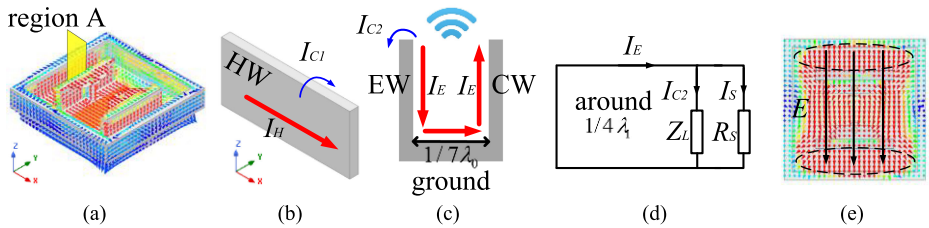

Fig. 2. (a) Simulated current distribution on the antenna at 60 GHz. (b) Currents on the HW. (c) Current distribution on the cross section of the radiating choke. (d) Equivalent circuit of the radiating choke. (e) E-field distributions of the antenna aperture at 60 GHz.

contribute to the radiation. The antenna is processed on low-cost, two-layer PCBs. The antenna also is cavity backed, and the realization of the MW in the PCB processing and its performance is discussed.

II. Antenna Evolution and Physics

The proposed antenna, shown in Fig. 1, is composed of a grounded WHEMS [21]–[24], the four edges of which are bent to the back plate, and a metal backing cavity. In Fig. 1(b), the grounded WHEMS is fed through two feeding rods connecting with the coupling aperture. Two bent walls of the WHEMS parallel to the *yz* plane are denoted the choking wall (CW). The walls of the backing cavity are denoted an E-wall (EW) and an H-wall (HW), where the two opposite walls normal to the *xz* plane are specified as the EW and the others HW. The model in Fig. 1(b) is realized in PCB processes shown in Fig. 1(c), where the antenna is composed of two, two-layer boards. One board on the top is the radiating part of the antenna with the other board realizing a SIW connected with WR12 waveguide for feeding. The dielectric constant of the substrate within the backing cavity is ε_1, which is set to 3.0 in the following electromagnetic simulations.

Simulated current distributions of the ideal model at 60 GHz are shown in Fig. 2(a). With a symmetrical structure and a balanced feed, the common-mode current is caused by the surface wave at the walls of the backing cavity. Current distributions on the HW are shown in Fig. 2(b), where I_H, parallel to the *xy* plane, is the copolarized current. I_{C1}, normal to the *xz* plane, is the common-mode current on the HW. Since I_{C1} is the cross-polarized current, it has limited effect on the radiation. As compared with I_{C1}, the choking current I_{C2}, the common-mode current on the EW, and also copolarized has more effect on the radiation, and is much more crucial.

To suppress I_{C2}, a structure composed of the EW, CW, and ground is introduced, the cross section of which is shown in Fig. 2(c), also the region A in Fig. 2(a). In the structure, one end of the EW and CW is short circuited by the ground with the other end open circuited. The wavelength in the substrate is

$$\lambda_1 = \frac{\lambda_0}{\sqrt{\varepsilon_1}} \tag{1}$$

where λ_0 is the wavelength in vacuum, andε_1 is the dielectric constant of the substrate within the backing cavity. As one end of the structure is short circuited, following the transmission line equation Z_L, the impedance at the open end, is

$$Z_L = jZ_0 \tan \beta l \tag{2}$$

where Z_0 is the characteristic impedance, β is the propagation constant, l is the height of the EW, and CW is $(1/4)\lambda_1$. Then, Z_L is ∞ calculated from (2), which is the principle choking mechanism of a current balun. The structure shown in Fig. 2(c) radiates due to the wide spacing $(1/7\lambda_0)$ between EW and CW and is a radiating choke with both common-mode-current suppression and radiating functions. The equivalent circuit of the radiating choke is shown in Fig. 2(d), where R_s is the radiation resistance and I_s is the current flowing in R_s. From the circuit, Z_L and R_s are in parallel. Thus, the choking condition of the radiating choke is modified from $Z_L = \infty$ to

$$Z_L \gg R_s. \tag{3}$$

The length of the radiating choke is no longer a quarter-wavelength, and the radiation results in a wide bandwidth choke.

Authorized licensed use limited to: HUNAN UNIVERSITY. Downloaded on March 04,2021 at 08:47:05 UTC from IEEE Xplore. Restrictions apply.

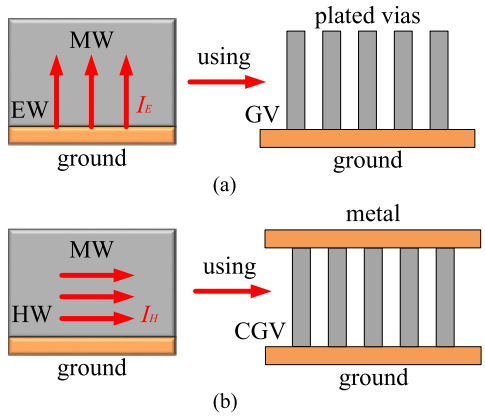

Fig. 3. Two ways to realize MWs in PCB processes in the proposed design. (a) Using GV to realize the MW with currents normal to the ground. (b) Using CGV to achieve the MW with currents parallel to the ground.

Evolved from the WHEMS antenna, which is a wideband radiating structure, the antenna itself has the potential for wideband performance. Shown in Fig. 2(d), an equivalent radiating resistance is terminated at the end of the radiating choke, which is a lossy loading for the antenna. The antenna achieves a wide bandwidth due to the decreasing of the Q-factor by the loading resistance, which is the radiating resistance contributing to the radiation.

Fig. 2(e) shows the E-field distributions of the antenna at 60 GHz, where the E-field in the aperture are in phase with almost the same amplitude. From the array theory, a high gain performance can be achieved by such uniform E-field distributions. Circled by black dotted lines, the radiating choke makes the E-field at both ends of the aperture more uniform and less tapered, which is the crucial point in reaching high gain.

III. Antenna Configurations and PCB Processing Discussions

Electrical connections in PCB processes are achieved through surface metal etching and plated vias. Thus, for a two-layer PCB, a MW can be constructed in two ways, as shown in Fig. 3, which are grounded vias (GV) and connected grounded vias (CGV). Perpendicular to the ground with one end open, the GV has good polarization characteristics for the currents perpendicular to the ground and rejects currents parallel to the ground. While the CGV supports currents parallel to the ground. As shown in Fig. 2(a), the polarizations of currents on the EW and HW are normal and parallel to the ground, respectively.

Shown in Fig. 3, based on the current polarization and the characteristics of the GV and CGV, an EW and HW are constructed using the GV and CGV, respectively. In Fig. 4(a), the ground plane of the proposed antenna is set at 20 mm $\times$ 20 mm to facilitate the observation of simulated currents and the later testing installation, as the diameter of the flange plate is 20 mm. Eight mechanical holes are set around the radiating part, where four small holes are for dowel pins and the others are for screws. The stack-up of the antenna is shown in Fig. 4(b), where the antenna consists of two PCBs. L1, L2, L3, and L4 are the metal layers of the PCB. The thickness of the two substrates S1 and S2 are 0.765 and 0.508 mm, respectively, where the substrate is realized in a Rogers 3003 material with a dielectric constant of 3.0. The dimension of the main radiator, shown in Fig. 4(c), is 4.60 mm by 4.72 mm, which are both less than a wavelength at 60 GHz. The diameter of the plated vias is 0.2 mm, and the pads for the GV are 0.5 mm in diameter, and have center-to-center distances of adjacent vias of 0.7 mm. The CGV does not have pads, and the center-to-center distances of adjacent vias is 0.3 mm. Thus, in Fig. 4(b), 8 vias and 13 vias comprise the EW and HW, respectively. The top and bottom views of Board 2, the SIW, are shown in Fig. 4(c) with the key parameters.

To further validate the design and the analysis mentioned above, the structure was simulated with different via termination schemes on the EW and HW. Current distributions on conductors were reviewed and shown to support the previously described current physics. Fig. 5 shows the simulated gain performance of the antenna in different wall cases. The GV and CGV were chosen to achieve the EW and HW of the proposed antenna, respectively, the common-mode current suppression of which was 3 dB or greater than in the other cases. The gain of the proposed antenna, with the least common-mode currents, at 60 GHz was 1.4–5.3 dB greater than the other three cases. Compared with large gain fluctuations in the other three cases, the proposed case realizes a relatively flat gain of 9–10 dBi over a 22% fractional bandwidth (60–75 GHz).

IV. Results and Discussion

The proposed antenna was measured in a far-field test system, with the R&S ZVA-Z90 vector network analyzer covering the band from 60 to 90 GHz. The prototype of the antenna, shown in Fig. 6, was manufactured in the PCB process following the dimensions and stack-up shown in Fig. 4. The two, two-layer PCBs were assembled through dowel pins and screws. Both the drilling accuracy of the PCB ($\pm$0.025 mm) and the mechanical accuracy of the dowel pins ($\pm$0.01 mm) determined the final assembly errors. The simulated and measured gains and $|S_{11}|$ are shown in Fig. 6. The simulated $|S_{11}|$ is below –10 dB over a frequency band from 60 to 79 GHz, where the measured curve has the same trend as the simulated curve. Discrepancies between measurement and simulation results result from both machining uncertainties of the PCB and the assembly errors. The plated vias near the coupling aperture are critical for the impedance performance. A $\pm$0.025 mm drilling error of PCB and the assembly error cause the final differences. A 9–10 dBi simulated gain is realized over 60–75 GHz, where the measured results are 8–10 dBi. The simulated directivity of the antenna is 9.3 dBi at 60 GHz, where the simulated radiation efficiency is 98%. The corresponding measured radiation efficiency defined by the measured gain over the simulated directivity is 95%. The simulated 3 dB beamwidth of both E- and H-planes are 70° and 56°, where the measured results are 50° and 45°, respectively. The simulated 6 dB beamwidth of both the E- and H-planes are 90° and 82°, where the measured results are 80° and 80°, respectively. The radiation pattern results are shown in Fig. 7, where the simulated results are in good agreement with the

Authorized licensed use limited to: HUNAN UNIVERSITY. Downloaded on March 04,2021 at 08:47:05 UTC from IEEE Xplore. Restrictions apply.

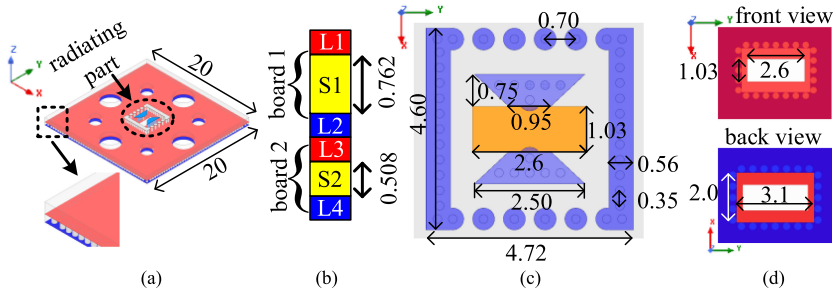

Fig. 4. Configurations of the proposed antenna. (a) Entire view. (b) Stack-up of the proposed antenna. (c) Top view of the radiating part of Board 1. (d) Top view and bottom view of the SIW part of Board 2. Dimensions are in millimeters.

TABLE I
COMPARISON WITH PUBLISHED AIP

Ref	Type	Bandwidth (GHz)	Gain (dBi)	Radiation aperture (mm^2) (elements)	Whole size (mm^2)	process
[16]	waveguide slot array with metal walls	2.0%(59.2-60.4)	20.6	17*22.5(4*8)	NA	LTCC
[17]	waveguide slot array with metal walls	7.7%(94.2-101.8)	17-19	20*10(4*4)	20*30	PCB
[18]	patch antenna with UC-EBG	5.4%(57.8-61.0)	17-18	18.5*18.5(4*4)	NA	LTCC
[19]	differential-fed patch with soft surface	11.7%(56.3-63.3)	18-19	14.5*15(4*4)	NA	LTCC
This work	WHEMS with GV and CGV walls	22.0%(60.0-75.0)	8-10	4.7*4.7(1*1)	20*20	PCB

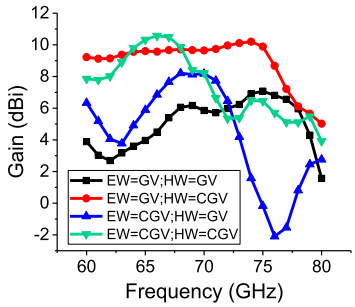

Fig. 5. Simulated gain results of the antenna in different wall cases.

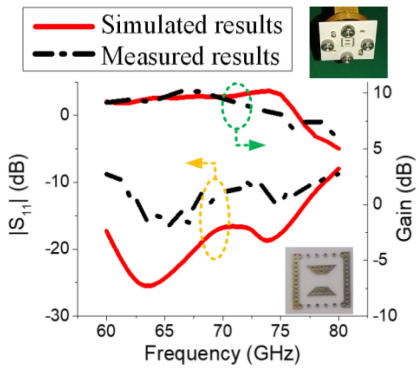

Fig. 6. Simulated and measured gain and $|S_{11}|$ results and photographs of the prototype.

measured results. The differences between the simulated and measured results may arise due to fabrication tolerances in the PCB process and measurement errors. A comparison is listed in Table I, between the proposed approach in this letter and other published ones listed in Section I. The proposed antenna has advantages of cost and bandwidth. The size of the radiation

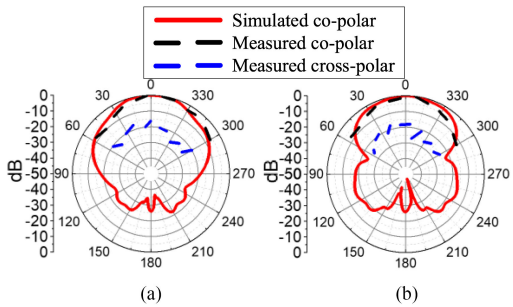

Fig. 7. Simulated and measured patterns at 60 GHz. (a) *H*-plane patterns. (b) *E*-plane patterns.

aperture has the potential to be optimized for various phased array applications.

V. CONCLUSION

A low-cost PCB manufactured antenna is proposed in this letter for 5G/6G AiP applications. A radiating choke, constructed through a grounded WHEMS and a backing cavity, is introduced, which not only suppresses the common-mode currents, but also contributes to the main radiation. Through simulations providing the currents on the enclosing walls, GV and CGV are applied to achieve the EW and HW, respectively. Finally, the antenna realizes a wide 22% gain bandwidth (60–75 GHz), and a relatively flat gain of 8–10 dBi within the band.

REFERENCES

[1] Q. Bi, "Ten trends in the cellular industry and an outlook on 6G," *IEEE Commun. Mag.*, vol. 57, no. 12, pp. 31–36, Dec. 2019.
[2] Y. Zhang, J. Deng, M. Li, D. Sun, and L. Guo, "A MIMO dielectric resonator antenna with improved isolation for 5G mm-wave applications," *IEEE Antennas Wireless Propag. Lett.*, vol. 18, no. 4, pp. 747–751, Apr. 2019.

Authorized licensed use limited to: HUNAN UNIVERSITY. Downloaded on March 04,2021 at 08:47:05 UTC from IEEE Xplore. Restrictions apply.

[3] S. F. Jilani, M. O. Munoz, Q. H. Abbasi, and A. Alomainy, "Millimeter-wave liquid crystal polymer based conformal antenna array for 5G applications," *IEEE Antennas Wireless Propag. Lett.*, vol. 18, no. 1, pp. 84–88, Jan. 2019.

[4] H. Y. Kim, T. H. Jang, H. H. Bae, and C. S. Park, "A 60 GHz compact multidirectional-beam antenna-in-package for mobile devices," *IEEE Antennas Wireless Propag. Lett.*, vol. 18, no. 11, pp. 2434–2438, Nov. 2019.

[5] F. Foglia Manzillo *et al.*, "A wide-angle scanning switched-beam antenna system in LTCC technology with high beam crossing levels for V-band communications," *IEEE Trans. Antennas Propag.*, vol. 67, no. 1, pp. 541–553, Jan. 2019.

[6] Y. P. Zhang and D. Liu, "Antenna-on-chip and antenna-in-package solutions to highly integrated millimeter-wave devices for wireless communications," *IEEE Trans. Antennas Propag.*, vol. 57, no. 10, pp. 2830–2841, Oct. 2009.

[7] Y. Zhang and J. Mao, "An overview of the development of antenna-in-package technology for highly integrated wireless devices," *Proc. IEEE*, vol. 107, no. 11, pp. 2265–2280, Nov. 2019.

[8] T. Zhang, L. Li, M. Xie, H. Xia, X. Ma, and T. J. Cui, "Low-cost aperture-coupled 60-GHz-phased array antenna package with compact matching network," *IEEE Trans. Antennas Propag.*, vol. 65, no. 12, pp. 6355–6362, Dec. 2017.

[9] P. Baniya, A. Bisognin, K. L. Melde, and C. Luxey, "Chip-to-chip switched beam 60 GHz circular patch planar antenna array and pattern considerations," *IEEE Trans. Antennas Propag.*, vol. 66, no. 4, pp. 1776–1787, Apr. 2018.

[10] Q. Liu *et al.*, "Reduction of EMI due to common-mode currents using a surface-mount EBG-based filter," *IEEE Trans. Electromagn. Compat.*, vol. 58, no. 5, pp. 1440–1447, Oct. 2016.

[11] A. E. Engin, N. Modi, and H. Oomori, "Stepped-impedance common-mode filter for differential lines enhanced with resonant planes," *IEEE Trans. Electromagn. Compat.*, vol. 61, no. 5, pp. 1457–1464, Oct. 2019.

[12] C. Jin, R. Li, S. Hu, S. Zhang, K. F. Chang, and B. Zheng, "Self-shielded circularly polarized antenna-in-package based on quarter mode substrate integrated waveguide subarray," *IEEE Trans. Compon., Packag., Manuf. Technol.*, vol. 4, no. 3, pp. 392–399, Mar. 2014.

[13] J. Park, D. Choi, and W. Hong, "Millimeter-wave phased-array antenna-in-package (AiP) using stamped metal process for enhanced heat dissipation," *IEEE Antennas Wireless Propag. Lett.*, vol. 18, no. 11, pp. 2355–2359, Nov. 2019.

[14] J. D. Kraus and R. J. Marhefka, "Baluns, etc.," in *Antennas for All Applications*. New York, NY, USA: McGraw-Hill, 2003, pp. 803–826.

[15] L. Wang, Y. Guo, and W. Sheng, "Wideband high-gain 60-GHz LTCC l-probe patch antenna array with a soft surface," *IEEE Trans. Antennas Propag.*, vol. 61, no. 4, pp. 1802–1809, Apr. 2013.

[16] H. Chu, J. Chen, and Y. Guo, "An efficient gain enhancement approach for 60-GHz antenna using fully integrated vertical metallic walls in LTCC," *IEEE Trans. Antennas Propag.*, vol. 64, no. 10, pp. 4513–4518, Oct. 2016.

[17] N. Ghassemi, K. Wu, S. Claude, X. Zhang, and J. Bornemann, "Low-cost and high-efficient w-band substrate integrated waveguide antenna array made of printed circuit board process," *IEEE Trans. Antennas Propag.*, vol. 60, no. 3, pp. 1648–1653, Mar. 2012.

[18] A. E. I. Lamminen, A. R. Vimpari, and J. Saily, "UC-EBG on LTCC for 60-GHz frequency band antenna applications," *IEEE Trans. Antennas Propag.*, vol. 57, no. 10, pp. 2904–2912, Oct. 2009.

[19] H. Jin, W. Che, K. Chin, G. Shen, W. Yang, and Q. Xue, "60-GHz LTCC differential-fed patch antenna array with high gain by using soft-surface structures," *IEEE Trans. Antennas Propag.*, vol. 65, no. 1, pp. 206–216, Jan. 2017.

[20] A. Rashidian, S. Jafarlou, A. Tomkins, K. Law, M. Tazlauanu, and K. Hayashi, "Compact 60 GHz phased-array antennas with enhanced radiation properties in flip-chip BGA packages," *IEEE Trans. Antennas Propag.*, vol. 67, no. 3, pp. 1605–1619, Mar. 2019.

[21] Z. Cai, Y. Qi, Z. Weng, W. Yu, F. Li, and J. Fan, "DC ground compact wideband omnidirectional vertically polarised slot loop antenna for 4G long-term evolution applications," *Microw., Antennas Propag.*, vol. 12, no. 7, pp. 1087–1092, Jun. 2018.

[22] Y. Xiao, Y. Qi, F. Li, J. Fan, W. Yu, and L. Lu, "Dual-band directional slot antenna for Wi-Fi application," *IEEE Trans. Antennas Propag.*, vol. 66, no. 8, pp. 4277–4281, Aug. 2018.

[23] L. Chi, Y. Qi, Z. Weng, W. Yu, and W. Zhuang, "A compact wideband slot-loop directional antenna for marine communication applications," *IEEE Trans. Veh. Technol.*, vol. 68, no. 3, pp. 2401–2412, Mar. 2019.

[24] L. Chi, Y. Qi, Z. Weng, W. Yu, F. Li, and J. L. Drewniak, "Directional antenna with consistent H-plane dual-band beamwidth for Wi-Fi applications," *IEEE Trans. Antennas Propag.*, vol. 67, no. 7, pp. 4495–4505, Jul. 2019.

Authorized licensed use limited to: HUNAN UNIVERSITY. Downloaded on March 04,2021 at 08:47:05 UTC from IEEE Xplore. Restrictions apply.